

# Enhanced thermomechanical functionality of a laser processed hybrid NiTi–NiTiCu shape memory alloy

M Daly<sup>1</sup>, A Pequegnat<sup>1</sup>, Y Zhou<sup>1</sup> and M I Khan<sup>1,2</sup>

<sup>1</sup> Centre for Advanced Materials Joining (CAMJ), Department of Mechanical and Mechatronics Engineering, University of Waterloo, 200 University Avenue West, Waterloo, ON, N2L 3G1, Canada

<sup>2</sup> Smarter Alloys Incorporated, MaRS Centre, South Tower, 101 College Street, Suite 200, Toronto, ON, M5G 1L7, Canada

E-mail: [m3daly@uwaterloo.ca](mailto:m3daly@uwaterloo.ca)

Received 21 November 2011, in final form 21 February 2012

Published 28 March 2012

Online at [stacks.iop.org/SMS/21/045018](http://stacks.iop.org/SMS/21/045018)

## Abstract

The exciting thermomechanical behavior of NiTi shape memory alloys (SMAs) has sparked significant research effort seeking to exploit their exotic properties. The performance capabilities of conventional NiTi offerings are limited, however, by current fabrication technologies. In this study, a high power density laser source was implemented to locally alloy Cu into a conventional NiTi material. The effects of laser processing created a localized NiTiCu ternary material domain which possessed a set of unique thermomechanical properties. The combined active responses of the laser processed hybrid NiTi–NiTiCu SMA represent an enhanced material functionality, which permits a multi-stage thermomechanical recovery and allows for unprecedented novel applications to be realized.

(Some figures may appear in colour only in the online journal)

## 1. Introduction

As one of the most recognizable and important shape memory alloys (SMAs), nickel–titanium (NiTi) is the focus of many recent research thrusts seeking to better understand and develop its functional properties. While NiTi has enjoyed relative success in many applications [1–3], next generation technologies require more precise control over its active thermomechanical properties. Furthermore, the controllability of conventional NiTi devices remains inhibited due to a well-known hysteresis associated with the mechanism responsible for shape memory and pseudoelastic behavior [4], namely the austenite–martensite phase transformation. Given that the thermomechanical properties of NiTi are extremely sensitive to the alloy processing history [5], traditional monolithic fabrication techniques cannot fully exploit its functional properties and are ultimately performance limiting. Recent investigations [6–8], however, have shown that laser processing can locally enhance the thermomechanical response of NiTi by altering the alloy composition within the

laser processing region. This technique, referred to as multiple memory material (MMM) processing, can be implemented to locally tune the thermomechanical properties by utilizing high power density energy sources, such as lasers [9, 10]. Using MMM processing, the performance capabilities of a conventional SMA can be expanded through localized control and customization of its thermomechanical response.

One established method to improve the thermomechanical behavior in NiTi is through the introduction of copper (Cu) into the binary system which results in the formation of the ternary NiTiCu intermetallic [11, 12]. Acting as a nickel substitutional, investigations have shown that relatively small amounts of Cu reduce the friction in the NiTi lattice and can therefore significantly narrow the transformation hysteresis loop [13, 14]. Furthermore, the addition of Cu to NiTi simultaneously modifies the thermomechanical behavior in the SMA by altering the Ti:(Ni, Cu) ratio. The purpose of the present work is to expand the functional properties of a conventional NiTi SMA by implementing MMM processing with a laser source to locally

alloy Cu into the parent base material. The resulting hybrid structure represents the first combination of binary NiTi and ternary NiTiCu SMA species within a monolithic alloy. Through laser processing operations, the functional properties of the conventional NiTi are augmented with a localized set of NiTiCu thermomechanical characteristics, therefore permitting a multi-stage SMA recovery with improved hysteresis.

## 2. Experimental details

Commercially available cold-rolled 400  $\mu\text{m}$  NiTi strip with a nominal composition of 50.8 at.% Ni and 49.2 at.% Ti was used as the reference alloy for this investigation. The as-received material was solution treated in a vacuum furnace at 800  $^{\circ}\text{C}$  for 3.6 ks followed by an argon gas quench. This heat treatment protocol is designed to achieve an annealed condition and remove any prior thermomechanical training. Prior to processing, the solutionized NiTi was chemically etched with a hydrofluoric–nitric acid solution to remove surface oxides, uniformly reducing the strip thickness to 370  $\mu\text{m}$ .

Localized alloying of the as-received NiTi base metal (BM) was achieved using a Miyachi Unitek model LW50-A pulsed Nd:YAG laser source with a nominal post-optic spot size of 600  $\mu\text{m}$ . In this study, laser energy is used to locally melt elemental constituents into the parent NiTi matrix. Chemically cleaned, high purity foils were used as elemental sources for laser processing operations. Given that solutionized NiTi exhibits shape memory characteristics in only the near-equiatomic range, a stoichiometric ratio of Ti was alloyed along with Cu in order to maintain Ti solubility, ensure substitutional competition of Ni and Cu, and eliminate the precipitation of unwanted Ni or Cu rich intermetallic compounds. In order to protect the laser processed zone (LPZ) from atmospheric contaminants, argon shielding was provided at a rate of 0.85  $\text{m}^3 \text{h}^{-1}$  (30  $\text{ft}^3 \text{h}^{-1}$ ). An illustration of the laser processing configuration and areas sampled for materials characterization is provided in figure 1. A sample region measuring approximately 1  $\text{cm} \times 1 \text{cm}$  was laser processed for this study. Full laser penetration through the sample cross-section was achieved to ensure proper melting. In its molten state, the LPZ was expected to rapidly homogenize due to Marangoni convection effects.

In order to confirm the presence of the NiTiCu intermetallic within the LPZ, the sample composition and crystal structure were investigated. A Jeol JSM-6460 scanning electron microscope (SEM) equipped with an INCA X-Sight 350 energy dispersive x-ray (EDX) analysis aperture was used for microscopy and chemical analysis of the BM–LPZ interface. As per a recent study by Undisz *et al* [15], a dilute HF etchant was used for microstructure analysis to limit surface pitting and avoid the formation of surface artifacts. Crystallographic data were collected from the BM and LPZ structures using micro-x-ray diffraction (XRD) analysis. XRD patterns were captured using a Rigaku SA-HF3 (1.54  $\text{\AA}$  Cu  $K\alpha$ ) x-ray source equipped with an 800  $\mu\text{m}$  collimator, operating at an excitation voltage of 50 kV. Specimens were carefully extracted from the LPZ bulk to prevent inadvertent sampling of the BM.

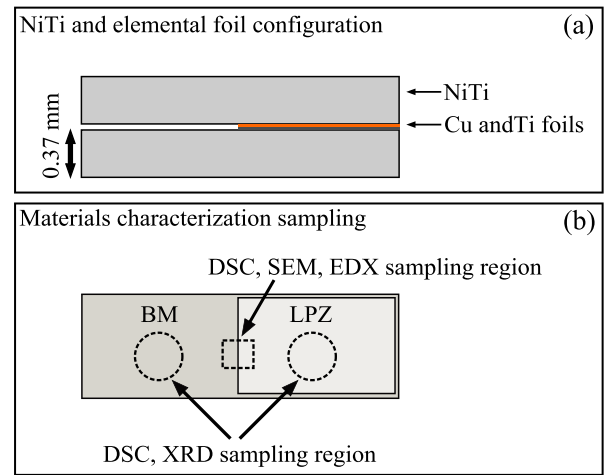


**Figure 1.** (a) Cross-sectional view (not to scale) of the laser processing configuration for the NiTi–NiTiCu SMA. (b) Top view of the laser processed specimen outlining the BM–LPZ interface and the bulk regions sampled for materials characterization testing.

Changes in phase transformation temperatures and thermal hysteresis in the hybrid NiTi–NiTiCu specimen were quantified via differential scanning calorimetry (DSC) instrumentation using a Thermal Analysis Q2000 acquisition system equipped with a refrigerated cooling unit. For data collection, a modified ASTM F2004-05 testing standard was followed. Heat flow was measured at a controlled heating and cooling rate of 5  $^{\circ}\text{C} \text{min}^{-1}$  in a range from  $-75$  to 120  $^{\circ}\text{C}$ . Austenite and martensite start and finish temperatures ( $A_s$  and  $A_f$ ,  $M_s$  and  $M_f$  respectively) were defined according to the ASTM standard and thermal hysteresis was calculated as the difference in temperature between peak heat flows in the heating and cooling curves.

The thermomechanical behavior of the NiTi–NiTiCu hybrid SMA was evaluated using an Instron model 5548 micro-tensile tester capable of a  $\pm 0.02 \mu\text{m}$  position resolution and  $\pm 0.5 \mu\text{m}$  measurement accuracy. In order to assess the thermomechanical response of the BM and LPZ, samples were cooled to below the  $M_f$  of the BM inside an environmental chamber and indented to a load of 100 N with a 1.6 mm (1/16 in) diameter spherical tip positioned in the tensile gripper jaws. After indentation, the samples were heated with a monotonic profile at a rate of 15  $^{\circ}\text{C} \text{min}^{-1}$  to above the  $A_f$  of the LPZ. During heating, a zero load condition was maintained on the crossheads and the indentation depth was continually monitored. The measured depth was then normalized against the  $J$  final indentation depth and correlated with the collected temperature data to provide an *in situ* assessment of the thermomechanical response. Specimen temperature was assessed using a resistance thermal device. The collected temperature measurements were digitally filtered using a low pass Butterworth algorithm to eliminate high frequency noise originating from the input AC line voltages. In order to visualize the changes in surface topography from the deformation and heating operations, a Veeco model WYKO NT1100 optical profiler with a depth resolution of 3 nm was used to image the indentation site of the LPZ at each stage of testing.

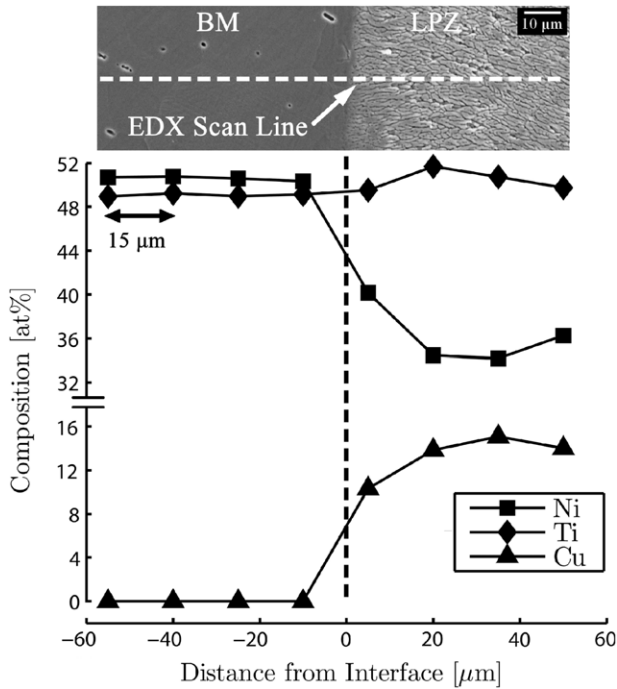


**Figure 2.** EDX line profile and microstructure cross-section along the BM–LPZ interface.

### 3. Results and discussion

#### 3.1. Detection of the NiTiCu intermetallic

The results from chemical analysis indicate that the Cu was well dispersed throughout the LPZ solidification structure. Due to the rapid cooling rates associated with laser processing, a distinct change in microstructure was observed between the LPZ solidification structure and equiaxed NiTi BM grains. As shown in figure 2, SEM imaging revealed dendritic grain growth and a typical solidification structure at the BM–LPZ interface which formed a well-defined boundary between material domains. An EDX line scan captured at the processing boundary showed a drastic rise in Cu content upon crossing the BM–LPZ processing line, quickly reaching bulk concentrations within a few  $\mu\text{m}$  of the interface. From further EDX analysis of the LPZ, the averaged bulk composition of the LPZ was determined to be  $\text{Ni}_{31.9}\text{Ti}_{52.1}\text{Cu}_{16}$  with a measurement standard deviation of 2 at.%. Although EDX results are expected to be accurate to  $\pm 1$  at.%, incomplete Marangoni mixing was likely the cause of minor inhomogeneities within the LPZ solidification structure.

While the results of chemical analysis detected Cu within the LPZ, it was necessary to verify the crystal structure of the NiTiCu intermetallic using XRD techniques. Results of the room temperature XRD analysis collected from the BM and LPZ are provided in figure 3. In order to clearly illustrate the subtle differences in crystal structures, a narrow  $2\theta$  range is presented. The obtained data agreed well with reference diffraction patterns for the NiTi and NiTiCu structures. The results indicated that the

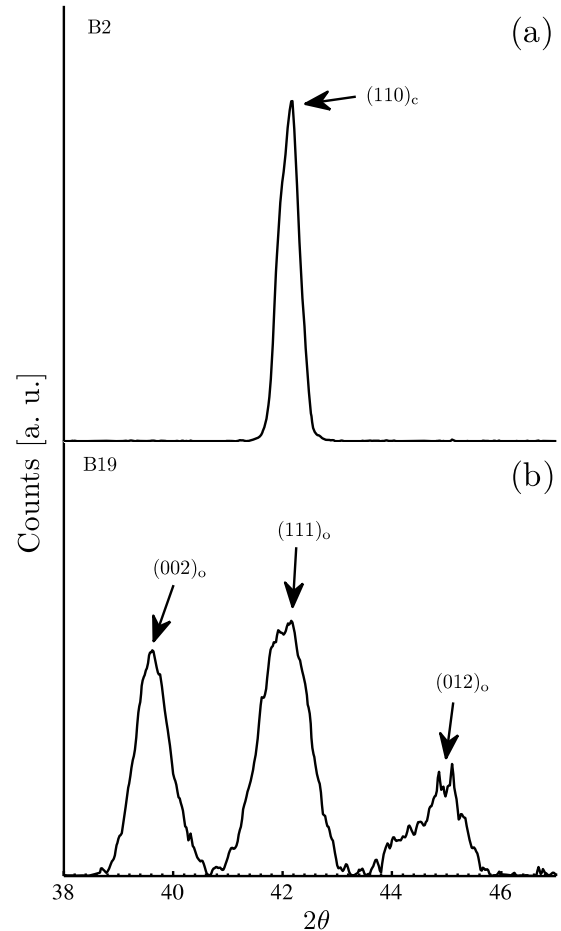


**Figure 3.** Room temperature XRD patterns of (a) B2 cubic BM austenite and (b) B19 orthorhombic LPZ martensite crystal structures.

BM possessed the expected cubic B2 austenite diffraction pattern, whereas the LPZ exhibited an orthorhombic B19 martensite structure [16]. It is well understood that Cu content drives competing orthorhombic and monoclinic martensite transformations in the NiTiCu system and therefore detection of a B19 orthorhombic structure as opposed to the typical B19' monoclinic crystal was not unexpected [14]. Furthermore, diffraction patterns from elemental Cu or Ti, common NiCu and TiCu compounds, or the parent NiTi alloy were not detected in the LPZ.

#### 3.2. Effects of laser processing on phase transformation temperatures and thermal hysteresis

The collected DSC scans for the NiTi BM and NiTiCu LPZ bulk are shown in figures 4(a) and (b), with the extrapolated transformation onset and finish temperatures and hysteresis provided in table 1. A considerable shift in phase transformation onsets was detected for the LPZ material domain, which increased well above the subzero temperatures observed in the BM. For example,  $M_s$  was found to increase by approximately  $100^\circ\text{C}$  in the NiTiCu domain when compared to the unprocessed NiTi. Furthermore, the results showed a significant reduction in transformation hysteresis of nearly

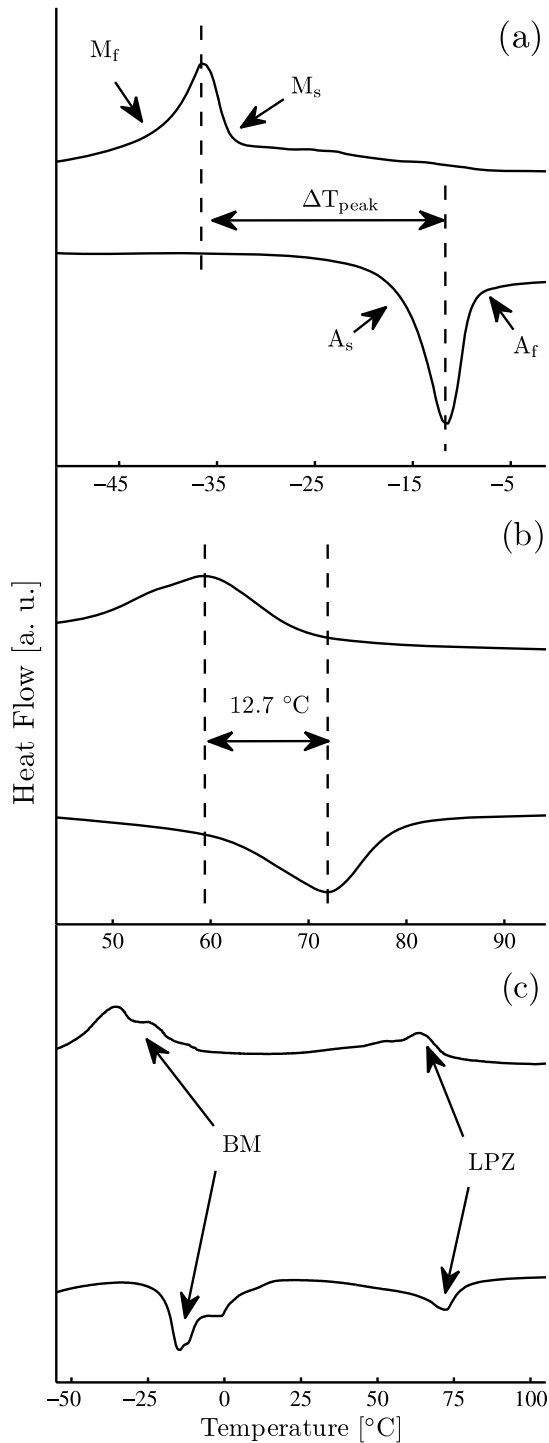


**Figure 4.** DSC scans of the BM (a) and LPZ (b) bulk, and BM-LPZ interface (c) showing altered hysteresis and shifted onset temperatures. The abscissae are offset in (a) and (b) to illustrate hysteresis narrowing.

50% between the BM and LPZ material domains. This drastic reduction of transformation hysteresis agreed very well with trends reported by Miyazaki and Ishida [13], who established a lower threshold for hysteresis in the NiTiCu system at approximately 12°C in chemistries greater than 10 at.% Cu. Increases in the DSC peak widths in the LPZ bulk were attributed to the minor inhomogeneity within the

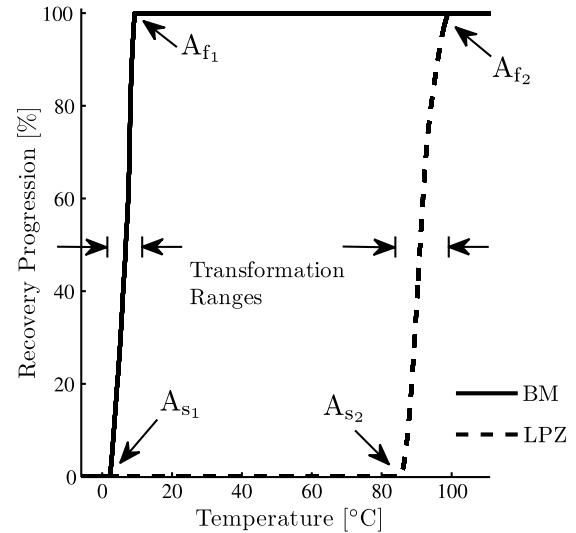


**Figure 5.** Thermomechanical recovery of the BM and LPZ as determined by indentation testing. BM and LPZ samples were each indented below the  $M_f$  of the BM and then heated monotonically to above the  $A_f$  of the LPZ.

**Table 1.** Phase transformation temperatures and hystereses (°C) for the BM and LPZ bulk.

Material domain	$A_s$	$A_f$	$M_s$	$M_f$	$\Delta T_{peak}$
BM	-16.1	-8.6	-33.0	-41.3	24.9
LPZ	59.5	79.3	69.9	44.7	12.7

solidification structure. Since the onset temperatures in NiTi SMA systems are extremely sensitive to the composition [17], minute variations within the LPZ created a wider thermal range in which the austenite-martensite phase transformation progressed [18]. In order to provide further evidence of hybrid functionality, a DSC scan of the BM-LPZ interface, illustrating both transformation characteristics, is provided in figure 4(c). The distortion of the transformation peaks is believed to be the result of internal stresses at the material interface.

### 3.3. Thermomechanical response of the NiTi-NiTiCu hybrid

The effects of laser processing have locally embedded a unique thermal response within the as-received NiTi BM. Prior to the processing operations, the NiTi BM was capable of only a single thermomechanical response which is dependent on its fabrication history. The introduction of Cu has altered the phase transformation temperatures and thermal hysteresis properties of the BM. A complementary change in thermomechanical response was therefore expected. The results from indentation testing confirmed the presence of two independent thermomechanical domains within the NiTi-NiTiCu SMA. As shown in figure 5, the collected data show independent recoveries of the BM and LPZ as they are heated through their respective phase transformation ranges ( $A_{s1}$ ,  $A_{f1}$  and  $A_{s2}$ ,  $A_{f2}$ ). The specific onset and finish temperatures observed in indentation testing differed

slightly from the extrapolated DSC measurements due to thermal sinking to the indentation head. Despite the relatively aggressive heating profile used during the thermal cycling of the indented specimens, the differences in transformation ranges between the BM and LPZ were well represented by the collected data and agreed well with the transformation peak widths observed in the DSC data.

In order to better visualize the recovery of the indented specimens, surface topographical profiles were collected at each stage of indentation testing for the LPZ. Given that the measurement range of the surface profilometer was limited to an area measuring  $300\ \mu\text{m} \times 225\ \mu\text{m}$ , a less aggressive indentation load of 15 N was used to ensure that the surface distortion was isolated to the measurement window. As shown in figure 6, the initially flat LPZ specimen was indented to a relative depth of approximately  $2\ \mu\text{m}$ . Upon heating the LPZ above its  $A_f$  temperature, the surface distortion directly beneath and peripheral to the indentation site recovered. As reported by Ni *et al* [19], a complete recovery of the pristine surface was not expected due to the complex strain distribution and material pile-up developed during the indentation operations.

### 3.4. Enhanced functionality of the NiTi–NiTiCu hybrid alloy

Comparison of the collected materials characterization analyses revealed that the binary parent NiTi structure has been reorganized into a ternary NiTiCu intermetallic within the LPZ. As shown in figures 4 and 5, laser alloying of Cu has created a new material domain with shifted phase transformation temperatures, therefore embedding a unique thermomechanical response within the LPZ. Furthermore, the transformation hysteresis was reduced in the LPZ, leading to improved SMA controllability. To the best of the authors' knowledge, this study represents the first example of a NiTi based SMA that possesses an enhanced thermomechanical functionality as the result of a locally embedded NiTiCu ternary system.

Laser processing of the as-received NiTi BM has created a hybrid SMA which possesses a customizable set of thermomechanical responses. From a device functionality perspective, unique shape memories can be triggered by progressively heating the NiTi–NiTiCu hybrid through its active thermal range. Unprecedented novel applications can therefore be realized by exploiting the multi-functional capabilities of this monolithic NiTi–NiTiCu SMA.

This study has focused on the enhanced thermomechanical behavior that was achieved through localized alloying of Cu into a parent NiTi alloy. However, the extent to which the laser alloying process can be used to enhance the functionality of conventional NiTi requires further investigation. Furthermore, the mechanical interactions between the processing domains and the base material are not fully understood. Future work will focus on understanding the micro-mechanical dynamics along the processing interfaces and characterization of complementary changes in pseudoelastic behavior. Investigation of other known ternary NiTi intermetallic species such as Pd, Hf, Zr, Cr, and Co is also planned in order to exploit other performance enhancing chemistries.

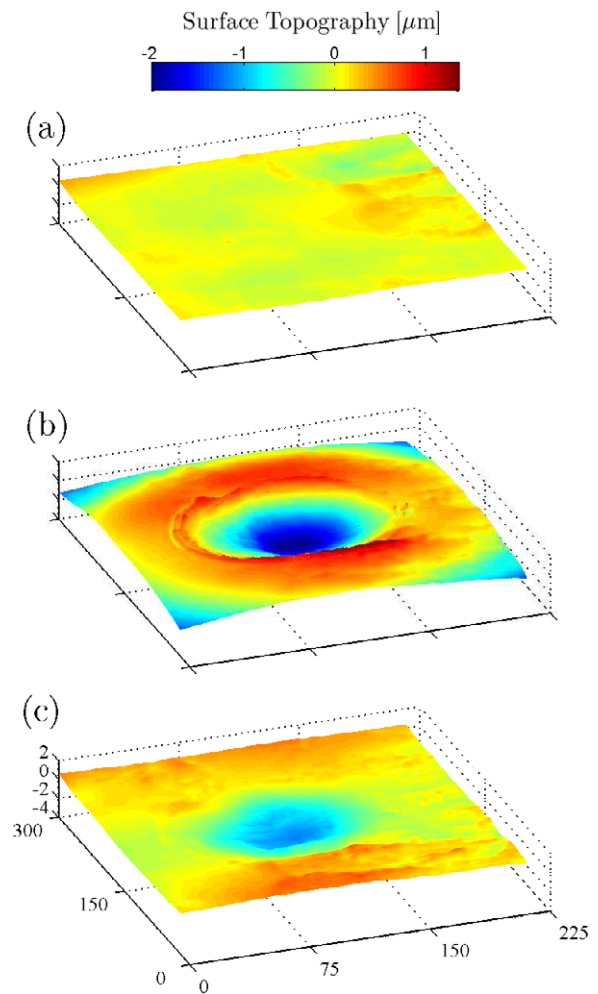


**Figure 6.** Surface topography of the indentation site of the LPZ at each stage of thermomechanical testing: prior to indentation (a); after indentation (b); and after heating above  $A_f$  (c). The axis labels are all in units of  $\mu\text{m}$ .

## 4. Conclusions

A novel laser processing technique has been used to locally alloy Cu into a NiTi SMA. The localized synthesis of a NiTiCu intermetallic was confirmed through chemical and crystallographic analyses. The results from DSC instrumentation showed that the NiTiCu material domain possessed a unique thermal behavior in comparison to the NiTi BM. Phase transformations in the LPZ were detected at over  $50\ ^\circ\text{C}$  above the sub-ambient austenite finish temperatures of the BM. Furthermore, the transformation hysteresis in the LPZ was found to be significantly reduced to  $12.7\ ^\circ\text{C}$ . Data captured from indentation testing indicated that the NiTi–NiTiCu hybrid SMA possessed two unique thermomechanical regimes, whose independent responses were a result of the composition differences between the BM and LPZ material domains. The combined thermomechanical responses of the NiTi–NiTiCu SMA hybrid represent a significant augmentation of traditional NiTi SMA capabilities and permit an enhanced functional material offering.

## Acknowledgments

The authors would like to acknowledge the support of the Natural Sciences and Engineering Research Council of Canada ([www.nserc.ca](http://www.nserc.ca)), Ontario Centres of Excellence ([www.oce-ontario.org](http://www.oce-ontario.org)), and the Canada Research Chairs Program ([www.chairs-chaire.gc.ca](http://www.chairs-chaire.gc.ca)).

## References

- [1] Fu Y, Huang W, Du H, Huang X, Tan J and Gao X 2001 *Surf. Coat. Technol.* **145** 107
- [2] Duerig T, Pelton A and Stöckel D 1999 *Mater. Sci. Eng. A* **273** 149
- [3] Hartl D and Lagoudas D 2007 *Proc. Inst. Mech. Eng. G* **221** 535
- [4] Funakubo H and Kennedy J 1987 *Shape Memory Alloys* (London: Gordon and Breach)
- [5] Otsuka K and Ren X 2005 *Prog. Mater. Sci.* **50** 511
- [6] Khan M I and Zhou Y 2010 *Mater. Sci. Eng. A* **527** 6235
- [7] Daly M, Pequegnat A, Khan M I and Zhou Y 2011 *Proc. ASME Conf. on Smart Materials, Adaptive Structures and Intelligent Systems (Phoenix, AZ, Sept. 2011)*
- [8] Pequegnat A, Vlasov M, Daly M, Khan M I and Zhou Y 2011 *Proc. ASME Conf. on Smart Materials, Adaptive Structures and Intelligent Systems (Phoenix, AZ, Sept. 2011)*
- [9] Khan M I and Zhou Y 2010 *Proc. Int. Conf. on Shape Memory and Superelastic Technologies (Pacific Grove, CA, May 2010)*
- [10] Khan M I and Zhou Y N 2011 Methods and systems for processing materials, including shape memory materials *World Patent Specification* 2011/014962
- [11] Mercier O and Melton K 1979 *Metall. Mater. Trans. A* **10** 387
- [12] Bricknell R, Melton K and Mercier O 1979 *Metall. Mater. Trans. A* **10** 693
- [13] Miyazaki S and Ishida A 1999 *Mater. Sci. Eng. A* **273** 106
- [14] Nam T H, Saburi T and Shimizu K 1990 *Mater. Trans. JIM* **31** 959
- [15] Undisz A, Reuther K, Reuther H and Rettenmayr M 2011 *Acta Mater.* **59** 216
- [16] Shugo Y, Hasegawa F and Honma T 1981 *Bull. Res. Inst. Miner. Dress. Metall.* **37** 79
- [17] Tang W 1997 *Metall. Mater. Trans. A* **28** 537
- [18] Frenzel J, Zhang Z, Somsen C, Neuking K and Eggeler G 2007 *Acta Mater.* **55** 1331
- [19] Ni W, Cheng Y and Grummon D 2002 *Appl. Phys. Lett.* **80** 3310